




Development of mesoporous ZSM-5 zeolite with microporosity preservation through induced desilication

Qian Ma¹, Tingjun Fu^{1,*}, Yujie Wang¹, Han Li¹, Liping Cui¹, and Zhong Li^{1,*} 

¹Key Laboratory of Coal Science and Technology of Ministry of Education and Shanxi Province, Institute of Coal Chemical Engineering, Taiyuan University of Technology, Taiyuan 030024, Shanxi, China

Received: 8 November 2019

Accepted: 19 May 2020

Published online:
2 June 2020

© Springer Science+Business
Media, LLC, part of Springer
Nature 2020

ABSTRACT

Alkali treatment is a widely used strategy to create mesopores for microporous zeolites to decrease the diffusion limitation in micropores. However, many of the micropore losses existed due to the uncontrollable destruction of framework. In this paper, a series of mesoporous ZSM-5 with well-maintained micropores was synthesized through induced desilication strategy. To induce the diffusion of alkali solution for the homogenizing desilication and mesopore formation, abundant and uniform small mesopores were firstly built for ZSM-5 by protective desilication in tetrapropylammonium hydroxide solution. The pore structure and acidity of the obtained ZSM-5 were characterized by XRD, TEM, N₂ physisorption, NH₃-TPD and Py-IR. Through induced desilication, the external surface area of obtained ZSM-5 increased from 42 m² g⁻¹ of parent ZSM-5 to 148 m² g⁻¹ and only 17% of micropore surface area was sacrificed, which was far lower than 37% of the loss in traditional NaOH treatment. Meanwhile, the strong acid sites were well preserved and the external acid sites were reduced. Compared with the sample treated by NaOH solution, the obtained catalyst exhibited higher catalytic stability and aromatics, especially PX selectivity. Good regenerated performance with long catalytic lifetime and high liquid hydrocarbon yield could also be found for the obtained catalyst. The strategy proposed in this paper is simple and ingenious in tailoring the porosity since it only relies on the desilication method, which is different from the usual coupling of dealumination and desilication.

Address correspondence to E-mail: futingjun@tyut.edu.cn; lizhong@tyut.edu.cn

Introduction

As a kind of synthetic crystalline aluminosilicates, ZSM-5 has been widely used for hydrocarbon synthesis and conversion [1, 2]. The zeolites feature of ZSM-5 is three-dimensional network including channels and cavities with micropore dimension, which endows it high surface area and pore volume for catalytic process [3]. For the ZSM-5 structure, aluminum atoms replace part of silicon atoms and produce charge defect. When H^+ are used to balance these charge defects, the zeolites can present acid sites [4]. It is noteworthy that only the acid sites in micropores can provide the function of shape selectivity for the above catalytic reactions [5, 6]. However, the narrow micropores of ZSM-5 ordinarily impose diffusion limitation to bulky reactants and products [7]. Particularly, the products trapped in micropores may undergo secondary reactions, like polymerization to form coke [8], eventually occupy the pore opening of micropores and poison the zeolites [9]. To conquer this restriction, long-term efforts have been devoted to decreasing the crystal size or introducing mesopores for the improvement of the diffusion in the bulk phase [10, 11].

Desilication is a versatile and reproducible methodology to introduce mesopores [12]. Conventional desilication of ZSM-5 uses NaOH solution as solvent to leach silicon to form mesopores. During the structural Si extraction process caused by OH^- , negatively charged AlO_4^- tetrahedra in framework repel OH^- because of their same charge and the hydrolysis of Si–O–Al bonds is hindered [13, 14]. Therefore, an appropriate SiO_2/Al_2O_3 ratio (50–100) is required for the introduction of obvious mesopores under a common condition [15]. For structures with high Al content, mesopores formation is hampered due to the limited silicon extraction. In contrast, for structure with low Al content, excessive internal desilication could occur because of insufficient shielding effect from AlO_4^- , resulting in formation of macropores or even hollow structure [16].

Importantly, a selective desilication mechanism exists during alkali treatment, which could increase the uncontrollability of desilication. The leaching of framework silicon atoms normally tends to occur at the defective sites, accompanied by the remove of internal Si–OH and increase in free Si–OH, where internal Si–OH represents internally located Si–OH

groups such as silanol nests and free Si–OH represents isolated Si–OH groups located on the external surface [17]. In the initial stage of desilication, some silicon atoms are removed under the guidance of defect sites to generate new mesopores. Then, the newly produced mesopores induce more OH^- to accumulate since the diffusivity coefficient could be increased by two to three orders of magnitude after the introduction of mesopores [18]. This fact essentially reduces the time and strength for the rest part of framework to be eroded, and the majority of mesopores are formed within a short period from the beginning during alkali treatment. Groen et al. [19] found that when ZSM-5 was treated with 0.2 M NaOH at 338 K, the mesopore surface area reached $180\text{ m}^2\text{ g}^{-1}$ after only 15 min. In short, control during the conventional desilication process is very low. Another serious challenge is the micropore loss of ZSM-5 in alkali treatment. Mochizuki et al. [20] treated ZSM-5 with 0.2 M NaOH for 1 h and found that the micropore surface area of the obtained ZSM-5 decreased from 375 to $291\text{ m}^2\text{ g}^{-1}$. Li et al. [21] increased the concentration of NaOH to 1 M, and the resulting zeolites suffered more severe micropore loss, whose micropore surface area decreased from 316 to $122\text{ m}^2\text{ g}^{-1}$. The severe micropore loss may play a negative part in shape selectivity of ZSM-5 because micropore space is indispensable for the formation of product during reaction [22].

In recent years, much attention has been given to the study of controllable desilication using external pore directing agents (protective desilication). Through this way, the surface protection can be formed and the uncontrolled desilication of the surface is inhibited, and finally, uniform mesopores are generated and the loss of microporous structure can be reduced. Wang et al. [23] added 0.01 M pyridine into 0.2 M NaOH solution and found that the addition of pyridine shielded the zeolite crystals from extensive dissolving by NaOH attacking. Thus, the micropore surface area of obtained ZSM-5 increased from 215 to $247\text{ m}^2\text{ g}^{-1}$ and the external surface area increased from 149 to $240\text{ m}^2\text{ g}^{-1}$ compared with the sample treated with NaOH solution. Quaternary ammonium base cation, such as TPA^+ (0.85 nm) and TBA^+ (1.07 nm), cannot enter the micropores (0.56 nm) of ZSM-5, but can absorb on the surface to shield the attack of OH^- during alkali treatment [24, 25]. Qiao et al. [26] described that when 0.2 M TPAOH was used to treat ZSM-5, the loss micropore

surface area of obtained ZSM-5 was low, which only decreased from 255 to 240 m² g⁻¹. Wan et al. [27] also treated ZSM-5 with 0.2 M TPAOH, and it was found that the obtained samples had uniform and abundant mesopores with a small size around 2–7 nm.

Herein, a new post-treatment strategy named induced desilication was proposed. Micro-ZSM-5 was treated with TPAOH solution to generate abundant small mesopores in bulky body, and the formed mesopores provided induced action for the next alkali treatment, thereby making the whole desilication process more uniform and controllable. The obtained ZSM-5 zeolites possessed both high mesoporosity and well-maintained micropores. Combined with a series of characterization, like XRD, TEM, N₂ physisorption, NH₃-TPD and Py-IR, the pore structure and acidic properties of the ZSM-5 zeolite obtained by induced desilication were investigated. The synthesized catalysts were applied in the MTA reaction, and the effects of the pore structure and acidity on the catalytic performance including catalyst stability and product selectivity were preliminarily studied.

Experimental section

Materials

The materials used are tetrapropylammonium hydroxide (TPAOH, Kermal, 25 wt.% aqueous solution), sodium hydroxide (NaOH, Tianjin Guangfu technology development Co. Ltd, 96%), ammonium chloride (NH₄Cl, Tianjin Guangfu technology development Co. Ltd, 99%), commercial ZSM-5 sample (SiO₂/Al₂O₃ = 50, Nankai University Zeolite Ltd) and tetraethyl orthosilicate (TEOS, Kermal, 98.0%). All reagents were used as received without further modifications.

Synthesis of hierarchical ZSM-5 via induced desilication

Commercial Na-ZSM-5 with SiO₂/Al₂O₃ ratio of 50 (Nankai University Zeolite Ltd.), denoted as Z5, was desilicated by 0.2 M TPAOH or NaOH solution, with a solid–liquid ratio of 33 mL/g. The alkali treatment was maintained at 353 K for 4 h under stirring with a stirring paddle and reflux conditions. The obtained slurry was centrifuged and washed with deionized

water until the pH value reached 7.0. After drying at 373 K overnight and calcining at 823 K for 6 h, samples of the first alkali treatment were obtained. For secondary alkali treatment, 5 g resulting powders were added into 75 mL alkaline solution at 353 K for 3 h under fierce agitation with a stirring paddle. Subsequently, the products were recovered by centrifugation, washing and drying. Finally, the zeolites were converted into H-form via three consecutive ion exchanges with 0.8 M NH₄Cl at 353 K for 3 h and the calcination at 823 K for 6 h. It should be noted that the concentration of OH⁻ and TPA⁺ for the second alkali treatment was systematically regulated. The selected concentration of OH⁻ was 0.1, 0.3 and 0.5 M. In order to study the effect of the introduction of TPA⁺ into 0.3 M OH⁻ solution on the mesopore formation, R value was defined as the molar ratio of TPA⁺/OH⁻ and the values were 0, 0.5 and 1, respectively. Refer to Table S1 for detailed conditions.

The prepared samples were named as Z5(a, b, c), where a and b referred to the R value of the first and secondary alkali treatments, respectively, and c represented the concentration of OH⁻ in the secondary alkali treatment. The samples only treated with 0.2 M NaOH solution was named Z5(0), and samples only treated with 0.2 M TPAOH solution was named Z5(1).

Post-treatment for silicalite-1 via induced desilication

Silicalite-1 with crystal size of 900 nm was synthesized in light of our previous work [28]. Raw materials were mixed with a molar composition of 1 SiO₂: 0.17 TPAOH: 4 EtOH: 46 H₂O and aged at 308 K for 5 h. The starting gel was then put into an autoclave for crystallization at 443 K for 72 h. After cooling, the slurry was centrifuged and washed. The as-synthesized sample was then dried overnight at 373 K followed by calcination at 823 K for 6 h and denoted as S900. 3 g S900 was added to 45 mL 0.2 M NaOH solution, and the suspension was heated to 353 K and kept 3 h under fierce agitation and reflux. The sample was centrifuged and washed thoroughly with deionized water until a pH of 7.0. Then, the product was collected and dried at 373 K overnight. The synthesized sample was named as S900-NaOH. S900-TPA was obtained under the same conditions aforementioned, except that the used solution was changed from NaOH to TPAOH solution. 2 g S900-TPA

was further desilicated by 30 mL 0.3 M NaOH at 353 K for 3 h. After being centrifuged and washed, the solid product was dried at 373 K overnight. The obtained sample was referred to S900-TPA-NaOH.

Characterization

X-ray diffraction (XRD) was employed to identify the phase and crystallinity. The patterns were recorded on Rigaku D/Max 2500 equipped with Cu K α ($\lambda = 1.54439 \text{ \AA}$) radiation under 40 kV and 100 mA with a scanning rate of $8^\circ/\text{min}$ in 2θ range of $5\text{--}50^\circ$. N₂ sorption of samples was carried out on a Beishide 3H-2000PS2 apparatus at 77 K after dehydrated at 523 K for 4 h. The surface area was measured by Brunauer–Emmett–Teller (BET) method. The pore size distribution was obtained by Barrett–Joyner–Halenda (BJH) method, and pore volume was derived from the t -plot method. Transmission electron microscopy (TEM) was acquired through JEM-2100F at the operation of 200 kV to determine the morphologies and structures of the samples. Before measurement, samples were dispersed with ethanol and then deposited on a porous carbon foil supported by a copper mesh. NH₃ temperature-programmed desorption (NH₃-TPD) was conducted on a Micromeritics Autochem II 2920 analyzer device with a thermal conductivity detector (TCD) to analyze acidity. Characteristically, 100 mg catalyst was pretreated at 823 K for 90 min in a He flow (50 mL min^{-1}). Thereafter, the sample was put into a gas mixture of 15 mol% NH₃ and 85 mol% He (50 mL min^{-1}) for sufficient NH₃ adsorption followed by cooling to 393 K. In the end, the sample was flushed in He stream (50 mL min^{-1}) at 393 K for 1 h to remove weakly adsorbed NH₃ and then the desorption temperature was increased from 393 to 823 K at a rate of 10 K min^{-1} . The Si and Al contents of ZSM-5 were measured by Epsilon 1 X-ray fluorescence spectrometer (XRF) produced by Panak Company at a voltage of 50 kV and a current of 100 μA . The range of test elements is Na-Am and ppm-100%. Tube anode is Ag target, and detector is SDD5. Quantitative standard is Omnia standard-free analytical procedure of Panak Company. Py-IR was used to obtain the ratio of Brønsted to Lewis acid sites (B/L ratio) of samples with a Bruker Tensor 27 spectrometer. Thermal gravimetric (TG) analysis was conducted on a STA449F3 analyzer at a heating rate of 10 K/min from room temperature to 973 K. The

amount of internal and external coke was calculated by TG and nitrogen adsorption result of the deactivated zeolites. Specifically, the internal coke content was calculated through multiplying the reduction of micropore volume by the density of coke, which is referred as 1.22 g cm^{-3} , and the external coke content is obtained by subtracting the internal coke content from the total coke content [29–31].

Catalytic test

Methanol-to-aromatic (MTA) reactions were carried out on a fixed-bed reactor. The main evaluation plan is that 0.5 g sieved ZSM-5 with 80–100 mesh and 2.5 g silica sand with 40–60 mesh were filled into stainless steel tubular and then activated in a N₂ flow at 723 K for 100 min. After activation, methanol was pumped into the gasification chamber at a flow rate of 0.105 mL/min by a micro-injection pump and was gasified at 513 K followed by mixing with a nitrogen flow of 35 mL/min before they entered into the reactor. During the reaction, the reaction temperature, pressure and methanol space velocity were controlled at 703 K, 0.5 MPa and $\text{WHSV} = 10 \text{ h}^{-1}$, respectively. In addition, in order to study the effect of methanol space velocity on the catalytic performance, the loading amount of catalyst was changed to 1.2 g, and the methanol injection rate was increased from 0.051 to 0.102 mL/min and then to 0.204 mL/min . The corresponding WHSV was 2, 4 and 8 h^{-1} . The regeneration of the deactivated catalyst was achieved by calcination at 600 °C for 5 h under air atmosphere. The regeneration performance of the deactivated catalysts was also studied at a condition of $T = 703 \text{ K}$, $P = 0.5 \text{ MPa}$ and $\text{WHSV} = 10 \text{ h}^{-1}$.

The liquid hydrocarbons were collected by the condensation unit and were analyzed through GC7890A gas chromatograph equipped with FID detector and PH-AL/S chromatographic column. Nitrogen was used as carrier gas. During the analysis, the temperature of the oven was first maintained at 313 K for 15 min and then increased to 473 K at a rate of 2 K/min . The calculation of product selectivity is based on area normalization method:

$$\text{Yield of liquid hydrocarbon (\%)} = \frac{m_{\text{hydro}}}{m_{\text{meth}}} \times 100\% \quad (1)$$

where m_{meth} denote the weight of methanol in feed, which was calculated by multiplying the injection rate of methanol by the injection time and methanol density, and m_{hydro} denote the weight of liquid hydrocarbon collected through the condensation unit.

Results and discussion

First desilication to construct uniform small mesopores

As shown in Fig. 1a, Z5(0) exhibited five typical diffraction peaks of MFI structure in ranges of 7° – 10° and 22.5° – 25° [31]. No impurities or amorphous phase were detected, indicating that the main crystalline framework was still maintained after alkali treatment. However, the diffraction peak intensity of Z5(0) decreased significantly and the relative crystallinity decreased from 100% of Z5 to 78% (Fig. 1a and Table S2), reflecting the partial destruction of the framework structure. H3-type hysteresis loop (Fig. 1b) of N_2 physisorption isotherms indicated that irregular mesopores were introduced. The pore size of the formed mesopores was around 10 nm, which can be reflected by BJH pore size distribution of Z5(0)

(Fig. 1c). The texture properties showed that the mesopore surface area of Z5(0) increased from $42 \text{ m}^2 \text{ g}^{-1}$ of Z5 to $141 \text{ m}^2 \text{ g}^{-1}$. Unfortunately, the micropore surface area decreased from 259 to $163 \text{ m}^2 \text{ g}^{-1}$ and the loss was 37%. TEM image also confirmed that large pores were formed in Z5(0) and the size of the pores was uneven, ranging from 6 to 15 nm (Fig. 2b).

For Z5(1) obtained by TPAOH treatment, the relative crystallinity was 85%, higher than that of Z5(0), indicating that the damage of framework structure of Z5(1) was less than Z5(0). Except type I isotherm, type IV isotherms were also observed and the hysteresis loop of Z5(1) was H_2 type, indicating the introduction of ink bottle-like mesopores. The external surface area of Z5(1) increased from 42 to $82 \text{ m}^2 \text{ g}^{-1}$, while the micropore surface area decreased from 259 to $237 \text{ m}^2 \text{ g}^{-1}$ and the loss was only 9% (Fig. 1d and Table S3). Besides, Z5(1) showed a sharp pore size distribution peak centered at $\sim 8 \text{ nm}$ (Fig. 1c), demonstrating the generation of small and uniform mesopores. This is because the hydrophobic TPA^+ tended to bind to hydrophobic silicate species on the zeolite surface, and large spatial resistance was generated because of the long hydrocarbon chain of TPA^+ . Thus, a shielding effect could be supplied to resist the attack of OH^- on zeolites. As a result, small

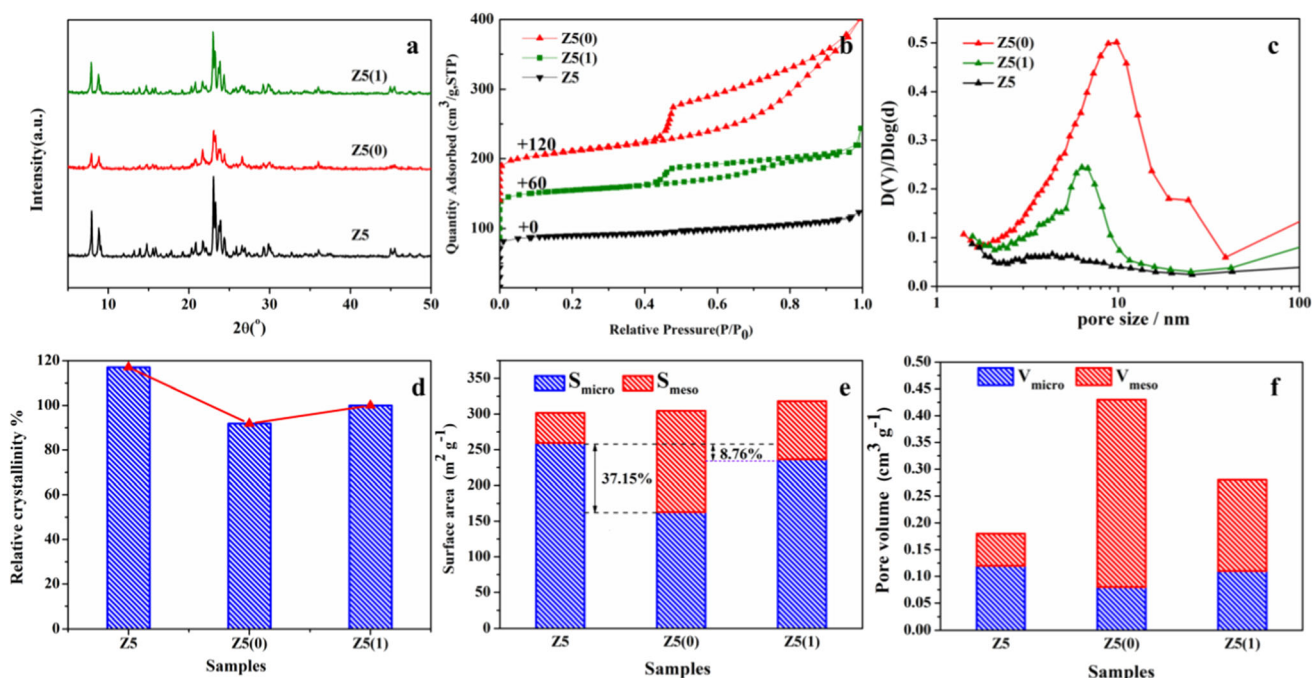


Figure 1 a XRD patterns, b N_2 isotherms, c BJH pore size distributions, d relative crystallinity and e, f texture properties of Z5, Z5(1) and Z5(0).

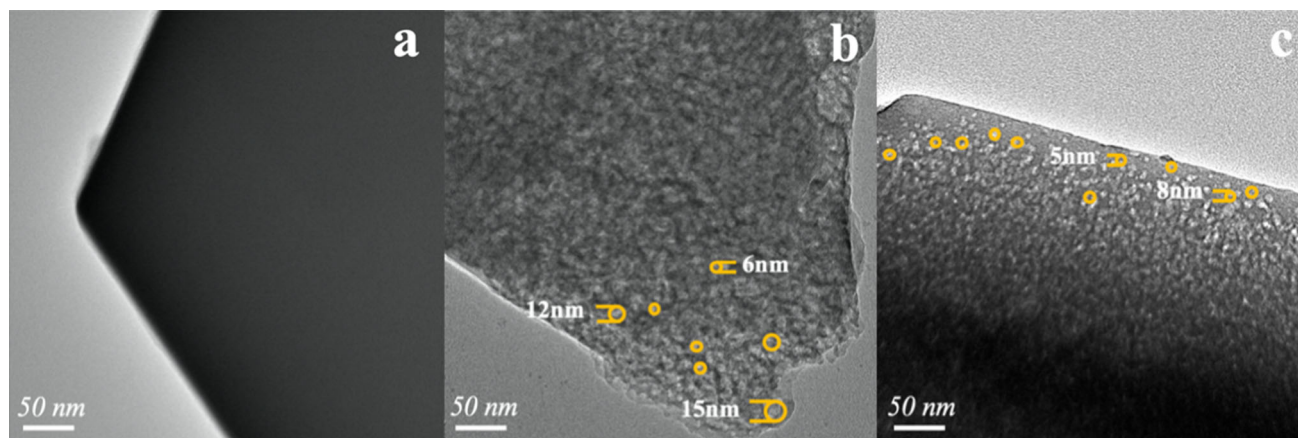


Figure 2 TEM images of **a** Z5, **b** Z5(0) and **c** Z5(1).

mesopores were fabricated along with the well-maintained micropores [32, 33]. TEM result (Fig. 2c) also reflected the uniformed mesopores with a size of about 5–8 nm. Considering the high microporosity and abundant small and uniform mesopores, Z5(1) was selected for further desilication to construct mesopores and study the induced desilication strategy.

Induced desilication based on preformed uniform small mesopores

Further desilication of Z5(1) was conducted with NaOH solution with diverse OH^- concentration. The relative crystallinity of Z5(1,0,0.1) increased from 85% of Z5(1) to 89%, and the mesopore volume increased from 0.17 to 0.22 $\text{cm}^3 \text{g}^{-1}$ (Fig. 3c and Table S3). This is because at a low OH^- concentration of 0.1 M, the main effect of OH^- was to remove debris left in the pore channel after first alkali treatment rather than attack framework forcefully. With increasing OH^- concentration to 0.3 M, the relative crystallinity of Z5(1,0,0.3) decreased to 80%, indicating further destruction of the framework. The mesopore surface area of Z5(1,0,0.3) increased by 82% compared with Z5(1), from 82 to 148 $\text{m}^2 \text{g}^{-1}$, while the micropore surface area decreased by only 9%, from 237 to 216 $\text{m}^2 \text{g}^{-1}$. This is far less than results reported in the literature that the loss of micropores was up to 25% even alkali treatment was performed at optimum $\text{SiO}_2/\text{Al}_2\text{O}_3$ ratio of 50–100 [15]. The results indicated that ZSM-5 with both high mesoporosity and well-maintained micropores could be obtained by induced desilication. When the OH^- concentration increased to 0.5 M, the mesopore surface area of Z5(1,0,0.5)

decreased to 138 $\text{m}^2 \text{g}^{-1}$, but the mesopore volume of Z5(1,0,0.5) increased to 0.52 $\text{cm}^3 \text{g}^{-1}$. It is inferred that some mesopores fused with surrounding mesopores. The pore size distribution of samples is shown in Fig. 3c. All curves showed a similar shape with a sharp peak. As the OH^- concentration increased, the position of these peaks shifted to the right and the distribution range became wider, suggesting that the introduced mesopores became larger and more inhomogeneous. It should be pointed out that Z5(1,0,0.3) exhibited a weak peak at 2–3 nm, but this did not represent the real mesopores and should be attributed to the “fluid-to-crystalline-like phase transition” of the adsorbed phase [34].

TEM images contributed mesoporosity-related messages in accordance with the pore structure described above. The morphology of Z5(1,0,0.3) was regular, suggesting no serious collapse of the framework after two consecutive alkali treatments. The rounded pores with the size centered at 8–10 nm were uniformly distributed, and most of them were independent each other (Fig. 4d). As for Z5(1,0,0.5), some large irregular holes caused by the fusion of small mesopores could be observed, which is consistent with the results of nitrogen adsorption.

The correlation between R value and the properties of alkali-treated samples was also investigated. With the increase in R value, the relative crystallinity of the samples increased (Fig. 5d), indicating that adding more TPA^+ in alkali treatment could provide better protection for the framework. When R value was increased to 0.5, the mesopore surface area of Z5(1,0.5,0.3) increased from 82 to 166 $\text{m}^2 \text{g}^{-1}$. This was because the competitive adsorption of Na^+ and

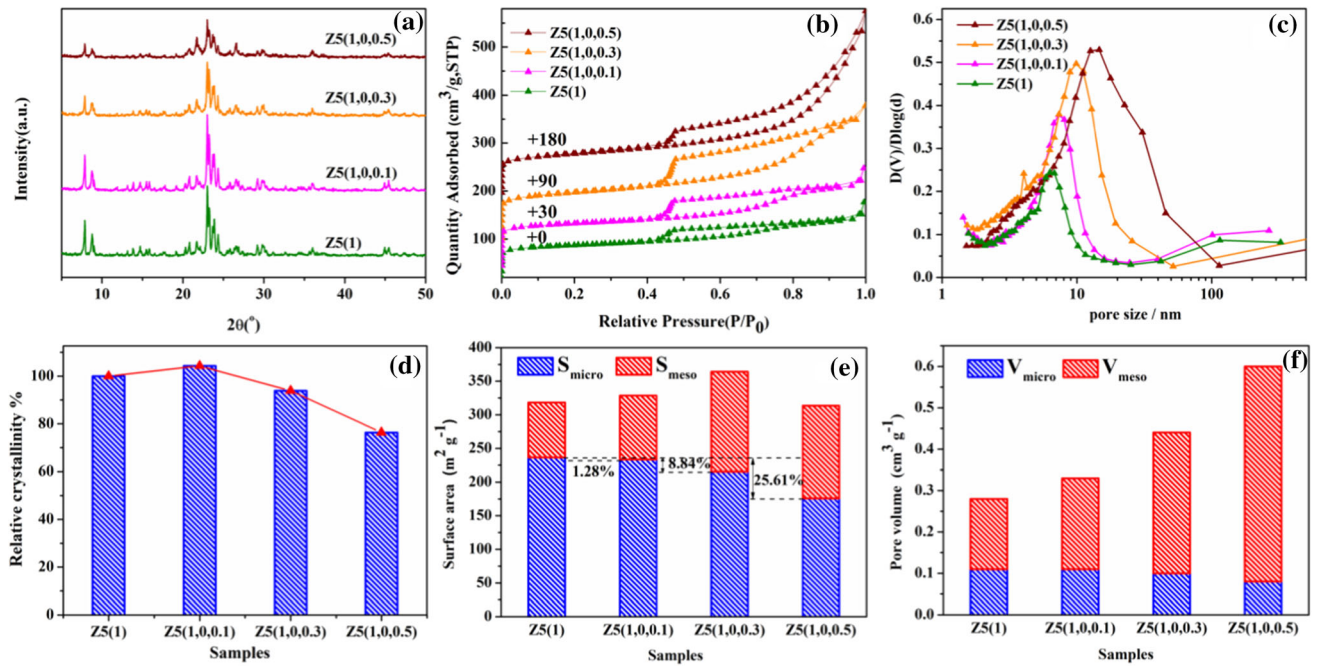


Figure 3 a XRD patterns, b N₂ isotherms, c BJH pore size distributions, d relative crystallinity and e, f texture properties of ZS(1), ZS(1,0,0.1), ZS(1,0,0.3), ZS(1,0,0.5).

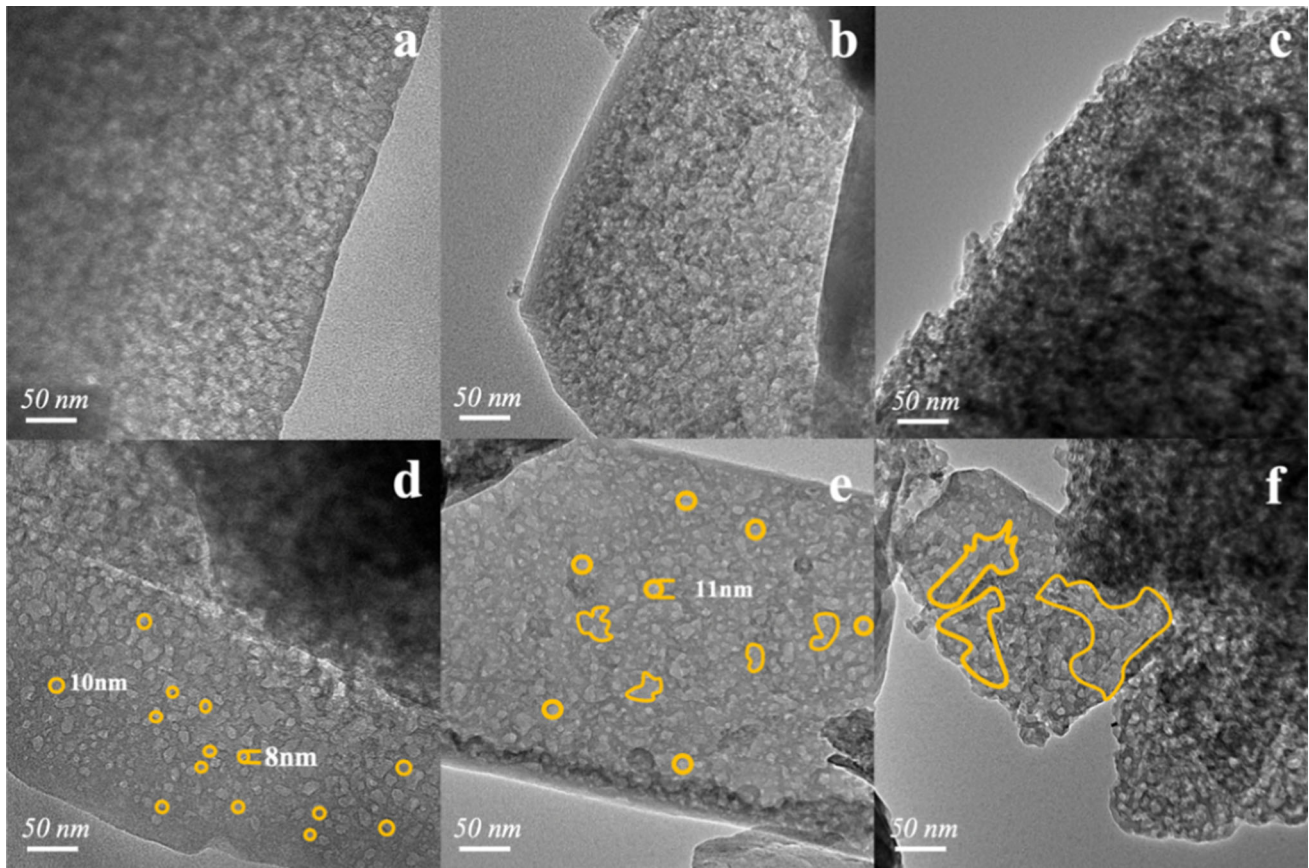


Figure 4 TEM images of a, d ZS(1,0,0.3), b, e ZS(1,0,0.5) and c, f ZS(0,0,0.3).

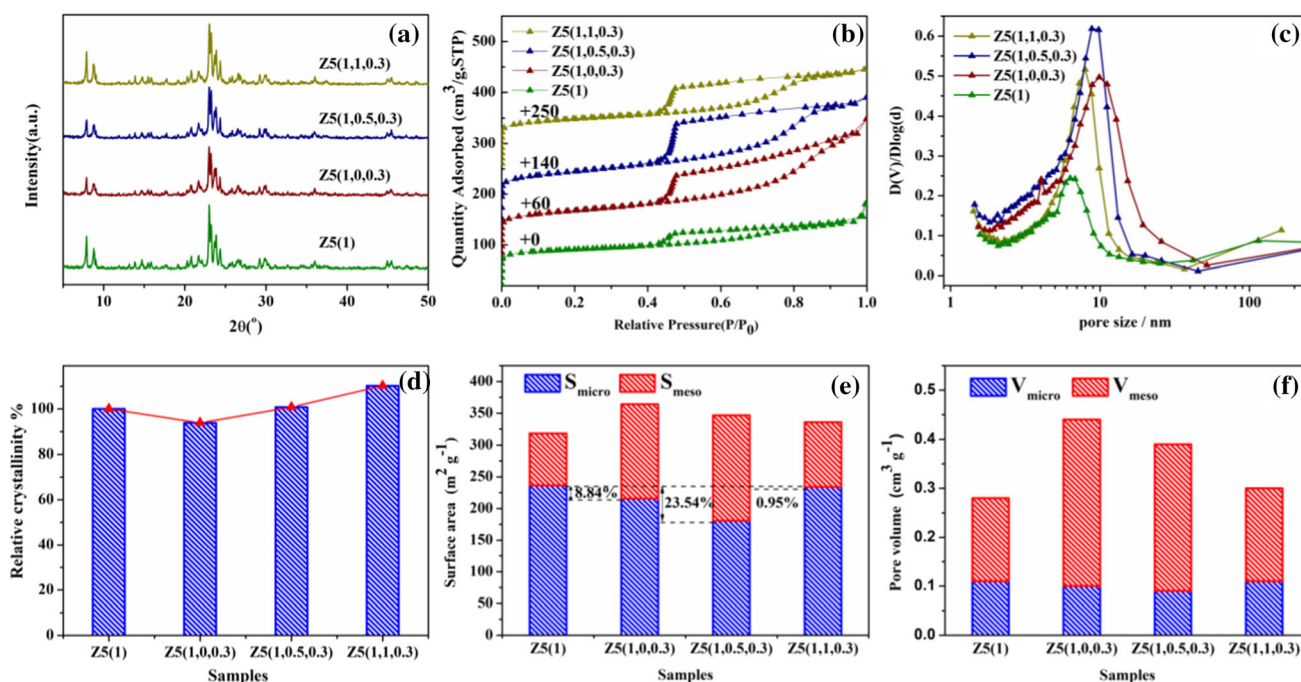


Figure 5 a XRD patterns, b N₂ isotherms, c BJH pore size distributions, d relative crystallinity and e, f texture properties of Z5(1), Z5(1,0,0.3), Z5(1,0.5,0.3), Z5(1,1,0.3).

TPA⁺ promoted desilication of ZSM-5 [27], and at the price, more micropores were sacrificed. When R value was increased to 1, the mesopore surface area of Z5(1,1,0.3) further decreased to 101 m² g⁻¹ and the mesopore volume decreased to 0.19 cm³ g⁻¹, indicating that strong surface protection was provided to inhibit mesopores formation during secondary TPAOH treatment [35].

A distribution map was depicted according to the micropore and mesopores surface area of the prepared samples (Fig. 6a). Samples at different locations on the map represent materials with different pore structures. Z5 was located at the bottom right corner, which represented micropore nature. After alkali treatment, the position of the samples moved to the left and upward, suggesting that introducing mesopores inevitably gave rise to the loss of micropores. Z5(0) was in the upper left corner of the map, indicating that the mesopore surface area of Z5(0) increased greatly and the microporous structure was seriously destroyed. The line between Z5 and Z5(0) divided the map into two parts. Z5(1) and its derived samples were located on the upper right of this line, indicating a better maintenance of the micropores for these samples. Specifically, the microporosity of Z5(1) was highest and the mesoporosity was lowest due to the overprotective effect of TPAOH during

desilication. Z5(1,0,0.1) and Z5(1,1,0.3) also failed to improve mesoporosity effectively owing to low concentration of OH⁻ or the excessive protection of TPA⁺. In comparison, the mesoporosity of Z5(1,0,0.3), Z5(1,0,0.5) and Z5(1,0,0.5) was significantly improved, and among them, the micropore surface area of Z5(1,0,0.3) was highest. This result illustrated that induced desilication could improve the mesoporosity of ZSM-5 on the basis of protecting the microporous structure.

Desilication mechanism

The above results preliminarily proved that the preformed uniform small mesopores had a positive induced effect on subsequent desilication. To further verify the conjecture, Z5(0) was treated with 0.3 M NaOH solution. The relative crystallinity of the obtained Z5(0,0,0.3) was only 67% (Table S2), and the loss of micropore surface area was 41% (Fig. 6b). Moreover, the fusion of mesopores was evident and some macropores were formed as shown in Fig. 4f. These results indicated that the large and uneven mesopores of Z5(0) cannot provide a positive and effective induction role in the subsequent desilication for the formation of mesoporous ZSM-5 with well protection of micropores.

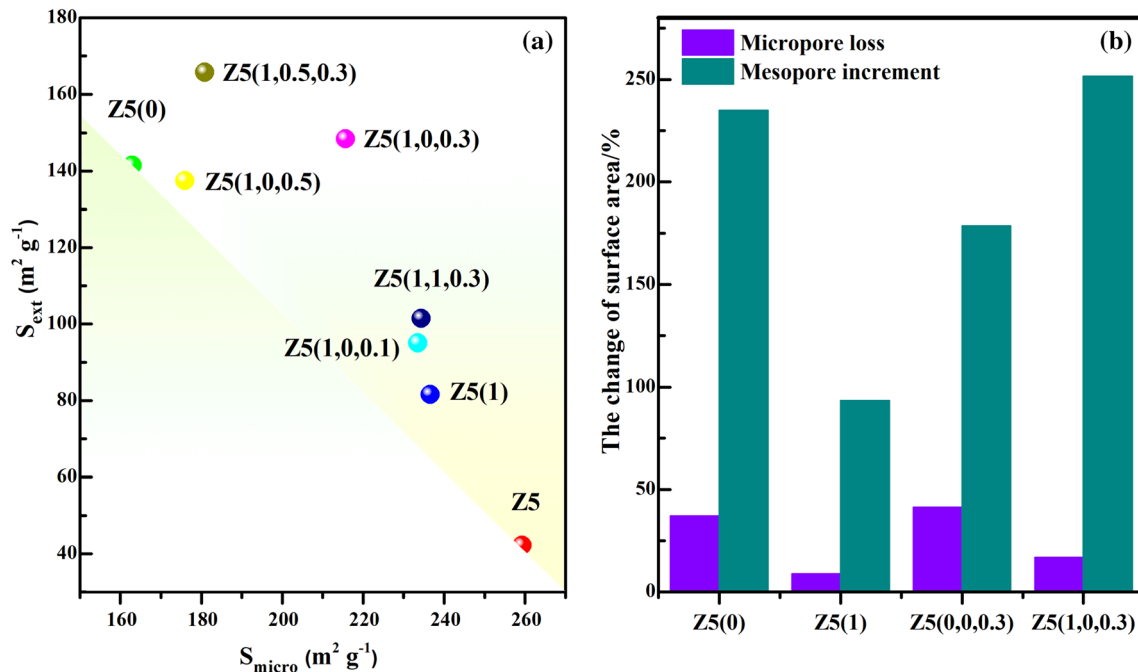


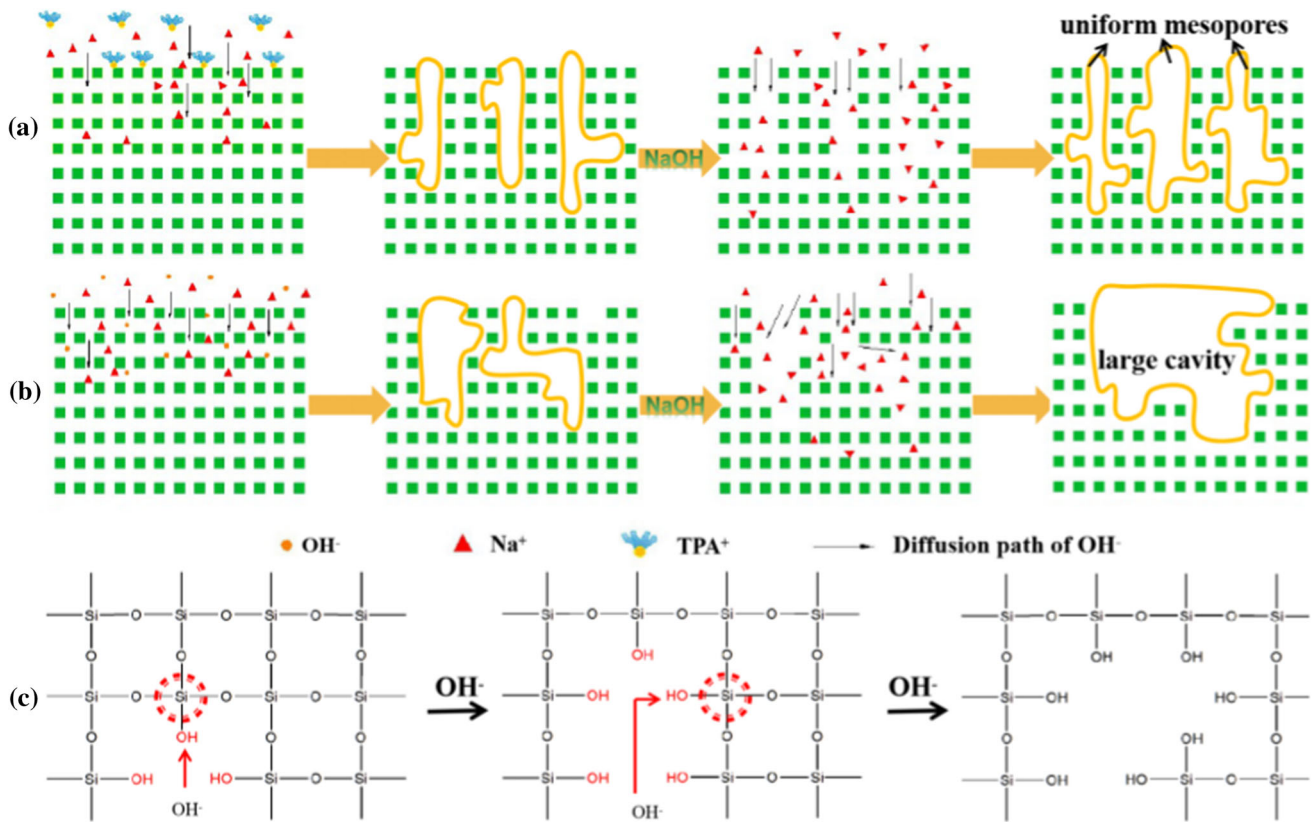
Figure 6 **a** Locations of samples on the map about the relationship of micropore and mesopore surface area and **b** micropore loss and mesopore increment of zeolites obtained by different treatments measured with Z5 as the reference.

The induced desilication mechanism can be described as Scheme 1a. Uniform small mesopores are successfully developed attributed to the protective effect of TPA^+ during first TPAOH treatment and guide the uniform diffusion of OH^- during the second alkali treatment. So the desilication becomes more mild and controllable, and the micropores are well maintained. In addition, uniform silanol nests are formed during TPAOH treatment [36], and during the second alkali treatment, these newly formed silanol nests play a guiding role for OH^- [17, 37], which makes the second alkali treatment more controllable (Scheme 1c). In comparison, traditional NaOH treatment could easily cause the formation of large uneven mesopores in a short time. These mesopores lead to the accumulation of alkali, which expand the mesopores and increase the heterogeneity of the mesopores. As a result, large holes even cavities are formed along with a strong damage of micropores (Scheme 1b).

The change of pore structure of silicalite-1 after alkali treatment could further verify the above induced desilication mechanism. S900 presented a regular coffin-like morphology with a crystal size of 900 nm (Fig. 7a), and a cicada-like morphology was observed for S900-NaOH, indicating that the intergrowth at edges of S900 takes over a dominant role

during NaOH treatment [38]. In comparison, TPAOH treatment resulted in a hollow-structured S900-TPA because of the surface protection of TPA^+ . When S900-TPA was further treated with NaOH solution, the cavity became larger and a cracked crystal edge was found although the damage was slighter than that for S900-NaOH. The special morphology of S900-TPA-NaOH indicated that in the second alkali treatment, the attack of OH^- was divided into two ways: One part of OH^- etched silicon from outside to inside; the other part diffused rapidly into cavity and then etched silicon from inside to outside.

The above results about the desilication of silicalite-1 intuitively proved the rationality of the induced desilication. Therefore, compared with couple strategy of dealumination and desilication by sequential steam or acid treatment and alkali treatment [39, 40], construction of uniform mesopores by simple desilication strategy is feasible. However, as described in Scheme 1, pre-constructed mesopores with different properties play different roles during secondary alkali treatment, so it is necessary to put SiO_2/Al_2O_3 ratio into consideration in order to build uniform small mesopores in the first alkali treatment and conditions should be explored to improve the efficiency of optimizing the pore properties.



Scheme 1 Induced desilication based on preformed **a** irregular large mesopores and **b** uniform small mesopores and **c** mesopore formation induced by defective sites.

The change of acidic properties during induced desilication

As shown in Table 1, the SiO₂/Al₂O₃ ratio in filtrate after NaOH treatment was 721, suggesting that the removed silicon was much more than that for aluminum. The removal of silicon decreased the SiO₂/Al₂O₃ ratio of Z5(0) from 44.5 of Z5 to 32.2 [41]. In comparison, the SiO₂/Al₂O₃ ratio in filtrate after TPAOH treatment was only 36, indicating that more aluminum was leached than Z5(0), and the SiO₂/Al₂O₃ ratio of Z5(1) was 44.5, even higher than that of Z5. When Z5(1) was treated with NaOH solution, the SiO₂/Al₂O₃ ratio of the obtained Z5(1,0,0.3) decreased to 38.1 for the further desilication. By comparison, the removal of silicon on the surface was inhibited when treated with TPAOH solution and the SiO₂/Al₂O₃ ratio of Z5(1,1,0.3) was increased to 41.2.

For the acidity of ZSM-5, as can be seen in Fig. 8a, all samples exhibited two NH₃ desorption peaks [42]. By Gaussian fitting, each NH₃-TPD curve was divided into three separated peaks, from which the amounts of weak, medium and strong acid sites

were, respectively, calculated. Z5 had the highest amount of strong acid sites of 0.51 mmol g⁻¹. NaOH treatment of Z5 seriously damaged microporous structure, and the amount of strong acid sites of Z5(0) decreased to 0.15 mmol g⁻¹, while for TPAOH treatment, the microporous structure was well maintained and the amount of strong acid sites of Z5(1) slightly decreased to 0.44 mmol g⁻¹. Further NaOH treatment of Z5(1) destroyed the microporous structure, and the amount of strong acid sites was reduced to 0.26 mmol g⁻¹. In comparison, TPAOH treatment of Z5(1) could maintain more micropores than Z5(1,0,0.3) and the amount of strong acid sites was 0.35 mmol g⁻¹. On the whole, there is a positive function between the amount of strong acid sites and relative micropore volume (Fig. 8b). Considering that the strong acid sites are active sites for methanol to aromatics reaction, the microporous structure should be protected as much as possible during the construction of mesopores through post-treatment process. In addition, part of the removed aluminum could reinsert in the framework during NaOH

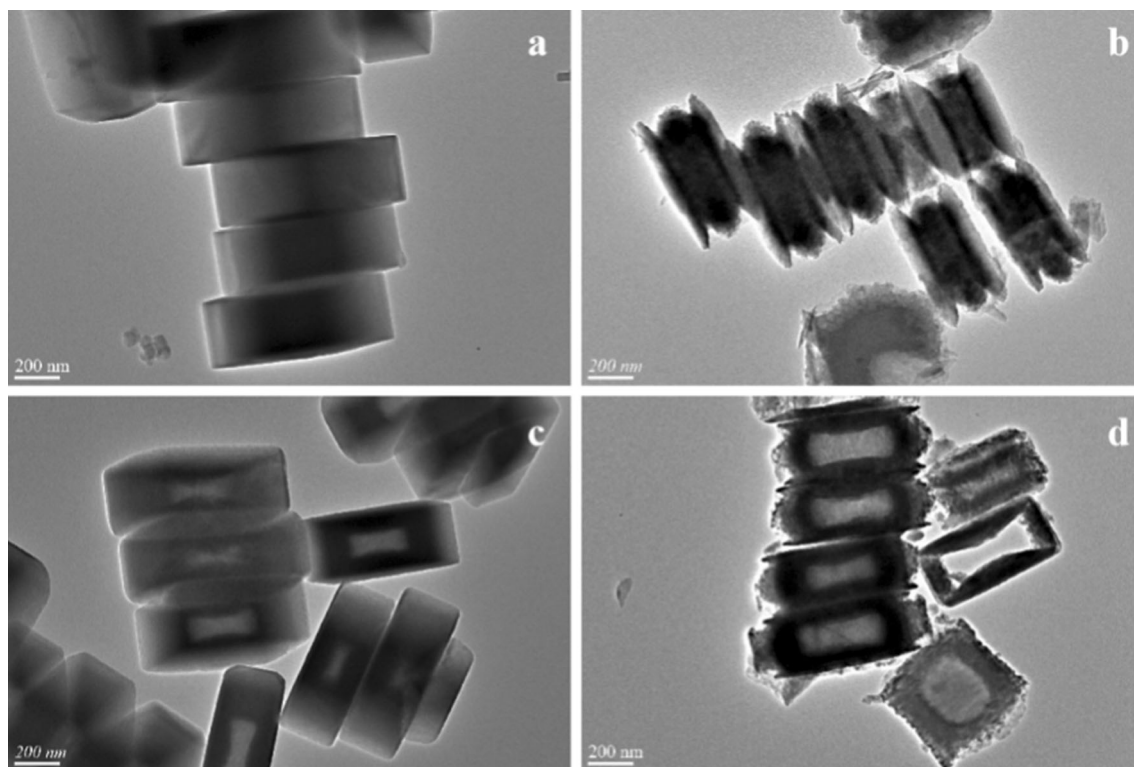


Figure 7 TEM images of **a** S900, **b** S900-NaOH, **c** S900-TPAOH and **d** S900-TPAOH-NaOH.

Table 1 SiO₂/Al₂O₃ and acidity properties of ZSM-5

Samples	SiO ₂ /Al ₂ O ₃ ^a		Acid amount (mmol g ⁻¹) ^b			
	Solid	Filtrate	Total	Weak	Medium	Strong
Z5	44.5	–	1.11	0.47	0.13	0.51
Z5(0)	32.2	721	0.93	0.35	0.44	0.15
Z5(1)	53.4	36	1.02	0.47	0.11	0.44
Z5(1,0,0.3)	38.1	–	0.90	0.47	0.17	0.26
Z5(1,1,0.3)	41.2	–	0.94	0.44	0.15	0.35

^aSiO₂/Al₂O₃ of bulky phase obtained by XRF

^bObtained by calculating the areas of three peaks obtained by the Gaussian fitting of two desorption peaks from NH₃-TPD

treatment, resulting in the increased amount of medium acid sites of Z5(0) compared with Z5 [19]. In comparison, when Z5 was treated with TPAOH solution, deposition of TPA⁺ on the surface limited the reinsertion of aluminum and no obvious increase in medium acid sites could be observed. The aforementioned XRF results of SiO₂/Al₂O₃ ratio in the two corresponding filtrate could also prove this result.

Py-IR results are shown in Fig. 9a, and the content of LAS and BAS is summarized in Table S4. The BAS

and LAS amounts of Z5 were 61.2 and 15.9 μmol g⁻¹, and B/L ratio was 3.9 (Fig. 9b). NaOH treatment destroyed the framework, and the BAS amount of Z5(0) decreased to 39.5 μmol g⁻¹. In addition, during NaOH treatment, part of leached aluminum reinserted into the zeolites and generated extra-framework Al. This reinsertion of Al increased LAS amount of Z5(0) to 31.9 μmol g⁻¹, and the B/L ratio of Z5(0) decreased to 1.2. In comparison, TPAOH treatment had less damage to framework, and BAS amount of Z5(1) increased from 39.5 μmol g⁻¹ of Z5(0) to 54.3 μmol g⁻¹. Meanwhile, the reinsertion of aluminum was limited to some extent during TPAOH treatment, and the LAS amount decreased to 20.7 μmol g⁻¹. Finally, the B/L ratio of Z5(1) increased from 1.2 of Z5(0) to 2.6. The second TPAOH treatment of Z5(1) further destroyed framework, and BAS amount of Z5(1,1,0.3) decreased to 40.6 μmol g⁻¹, while LAS amount increased to 26.2 μmol g⁻¹, so B/L value decreased to 1.5. For Z5(1,0,0.3), the framework damage was aggravated and the production of extra-framework aluminum was also increased compared with that of Z5(1,1,0.3); therefore, the BAS amount decreased to

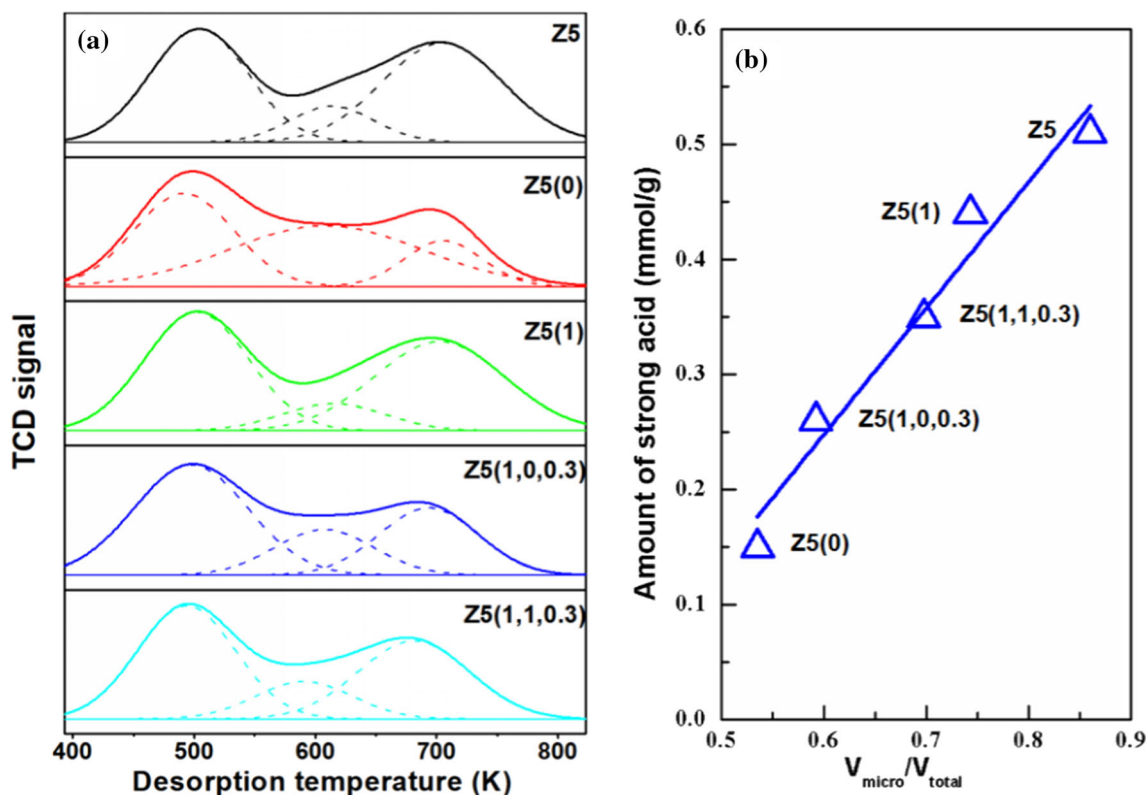


Figure 8 a NH₃-TPD profiles of various ZSM-5 zeolites and b the amount of strong acid versus relative micropore volume.

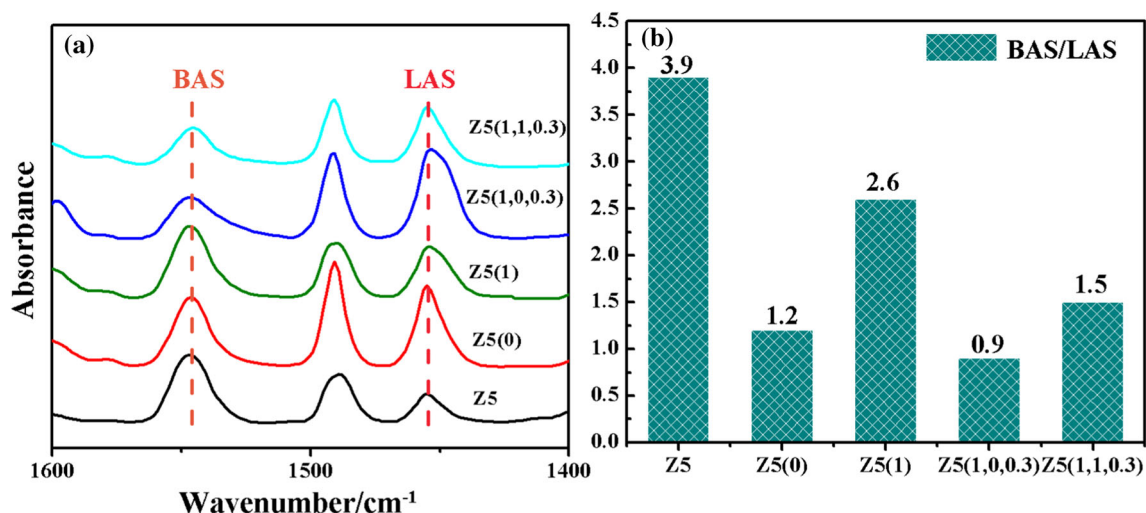


Figure 9 a Py-IR spectra and b the B/L ratio of various ZSM-5 zeolites.

35.1 $\mu\text{mol g}^{-1}$, while LAS amount increased to 38.3 $\mu\text{mol g}^{-1}$ and B/L ratio further decreased to 0.9.

MTA performance

MTA performance result is shown in Fig. 10a. On the whole, the lifetime of the sample increased with the

increase in external surface area, while decreased with the increase in amount of strong acid sites (Fig. 10b). Specifically, the lifetime of Z5 was only 10 h and the yield of liquid hydrocarbon was only 12.6%, which is calculated by Eq. (1). Its strong acid sites accelerated the formation of coke, and the coke could not easily migrate to external surface due to the

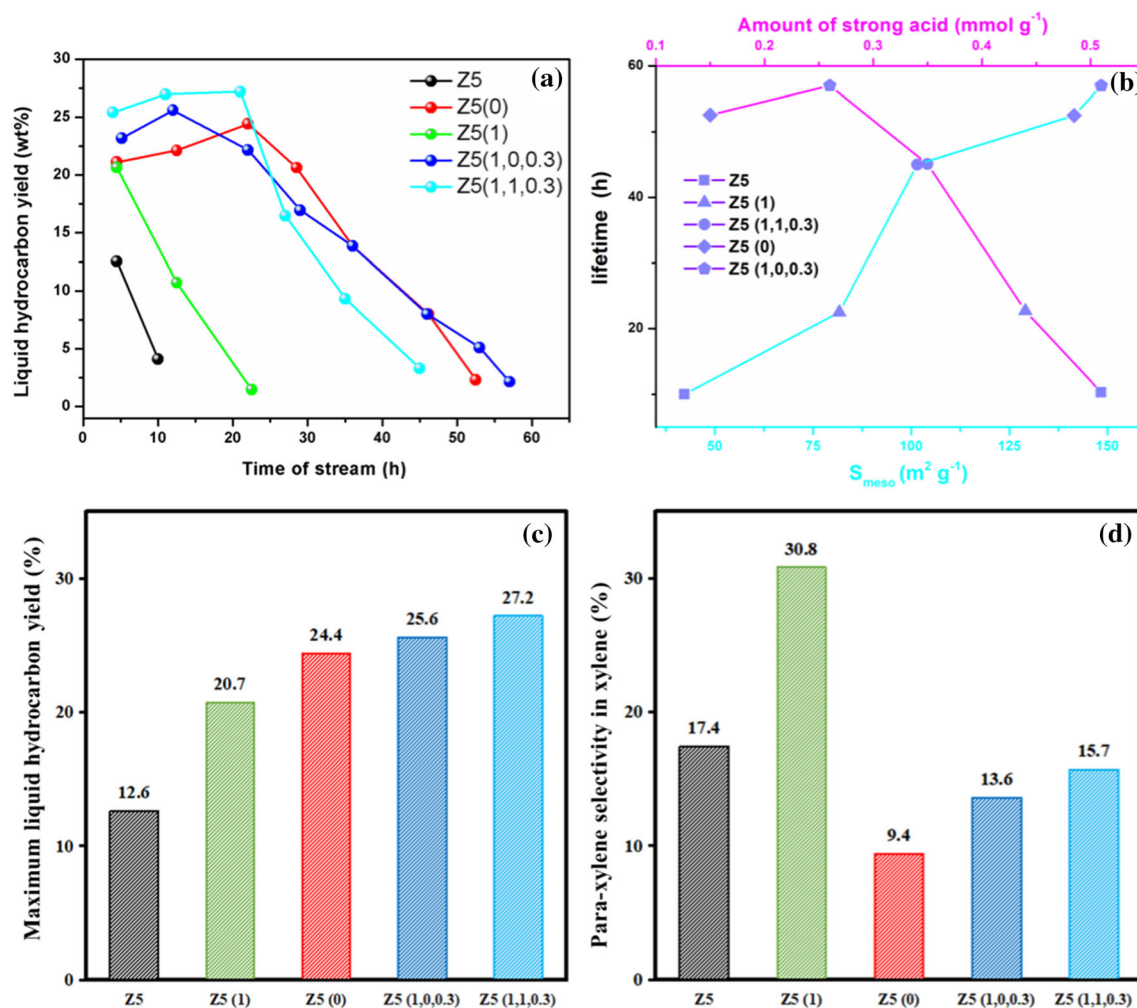


Figure 10 **a** Liquid hydrocarbons yield with the time on stream (reaction condition: $T = 703$ K, $P = 0.5$ MPa and the $WHSV = 10$ h^{-1}), **b** relationship between lifetime and the

amount of strong acid sites and mesopore surface area and **c**, **d** maximum liquid hydrocarbon yield and para-xylene selectivity in xylene of samples.

intrinsic micropores and then block the diffusion exits and gradually cover the active acidic sites [43]. The introduction of small mesopores in Z5(1) reduced the diffusion limitation of micropores [44], and the amount of strong acid sites decreased to 0.44 $mmol g^{-1}$, so the lifetime increased from 10 h to 22.5 h. Moreover, the product molecules could diffuse to the outside more easily and the yield of liquid hydrocarbons increased to 20.7%. In comparison, mesoporosity of Z5(0) was further increased and diffusion of bulky products was improved. Therefore, its lifetime increased to 52.5 h and the liquid hydrocarbon yield further increased to 24.4%. TPAOH treatment of Z5(1) introduced more mesopores into Z5(1,1,0.3), and the amount of strong acid sites decreased to 0.35 $mmol g^{-1}$ compared with

Z5(1); accordingly, the lifetime increased to 45 h. When Z5(1) was treated with NaOH solution, the mesoporosity of Z5(1,0,0.3) was further enhanced and the amount of strong acid sites decreased from 0.44 to 0.26 $mmol g^{-1}$, so the lifetime of Z5(1,0,0.3) increased to 58 h. It is worth noting that the liquid hydrocarbon yield of Z5(1,1,0.3) was higher than that of Z5(1,0,0.3), which was attributed to the well-maintained microporous structure and high amount of strong acid sites that provided more active sites for MTA reaction [45].

The PX selectivity (para-xylene selectivity in xylene isomers) of Z5 was 17.4% (Fig. 10d). NaOH treatment destroyed micropores of Z5(0) and decreased the shape selectivity for PX. In addition, the reinserted aluminum atoms generated more external acid sites and increased the occurrence of the isomerization of

xylene [36, 46], so the PX selectivity of Z5(0) decreased to 9.4%. In comparison, the well microporous structure of Z5(1) ensured better shape selectivity for PX [47]. Meanwhile, during TPAOH treatment, the reinsertion of aluminum and generation of external acid sites were inhibited, and PX selectivity of Z5(1) increased to 30.8%. Further TPAOH treatment of Z5(1) destroyed part of micropores and increased reinserted aluminum, so the PX selectivity of Z5(1,1,0.3) decreased to 15.7%, while for Z5(1,0,0.3), the micropores were further damaged and more aluminum atoms were reinserted, and its PX selectivity decreased to 13.6%. In summary, two considerations need to be noted when alkali treatment was applied to introduce mesopores into the bulk of ZSM-5. The first point is that the micropores should be protected as much as possible to ensure the selectivity of the target product. Another is that the acidity of zeolites should be properly reserved to ensure high product yield.

TG curves of deactivated samples are shown in Fig. 11a. The total coke content and formation rate were calculated through the weight loss in the stage of 400–650 °C, and the results are shown in Table 2. Parent Z5 presented a high coke formation rate of $8.38 \times 10^{-3} \text{ g g}^{-1} \text{ cat h}^{-1}$ for strong acidity and natural microporous structure. The formed coke quickly covered the acid sites and deprived them of catalytic activity, and the coke content of Z5 was only $0.08 \text{ g g}^{-1} \text{ cat}$. After the introduction of small mesopores into the bulk of Z5(1), the coke precursors formed inside the micropores could diffuse to the external surface more easily, and the amount of strong acid sites decreased to 0.44 mmol g^{-1} , and coke formation rate decreased to $5.34 \times 10^{-3} \text{ g g}^{-1} \text{ cat h}^{-1}$. In addition, the increased external surface of Z5(1) provided higher carbon capacity, and the coke content increased to $0.12 \text{ g g}^{-1} \text{ cat}$ [48, 49]. Compared with Z5(1), the larger mesopores in Z5(0) and the decreased strong acid sites further slowed down the coke formation rate to $3.24 \times 10^{-3} \text{ g g}^{-1} \text{ cat h}^{-1}$. The external surface area of Z5(0) increased to $141 \text{ m}^2 \text{ g}^{-1}$ and the coke content increased to $0.17 \text{ g g}^{-1} \text{ cat}$. The mesopores surface area of Z5(1,0,0.3) was increased compared with Z5(1), and the amount of strong acid sites decreased, so the coke formation rate of Z5(1,0,0.3) reduced to $3.62 \times 10^{-3} \text{ g g}^{-1} \text{ cat h}^{-1}$ and the coke content increased to $0.21 \text{ g g}^{-1} \text{ cat}$. In comparison, the mesopores of Z5(1,1,0.3) were smaller than Z5(1,0,0.3) and the amount of strong acid sites

increased to 0.35 mmol g^{-1} ; therefore, the coke content decreased to $0.16 \text{ g g}^{-1} \text{ cat}$ and the coke formation rate increased to $3.64 \times 10^{-3} \text{ g g}^{-1} \text{ cat h}^{-1}$.

The spent catalysts were also characterized by N_2 physisorption analysis (Fig. 11b). All the spent catalyst exhibited remarkable decline in adsorption capability at the low relative pressure region, suggesting the micropores were significantly occupied by coke. In order to further investigate the locations of coke, we defined the $R_{V_{\text{micro}}}$ and $R_{V_{\text{meso}}}$ to denote the relative variation degree of micropores and mesopores volume. $R_{V_{\text{micro}}}$ and $R_{V_{\text{meso}}}$ represent the proportion of the change of micropore or mesopore volume to the change of total pore volume, respectively (Fig. 11d). The $R_{V_{\text{micro}}}$ value of Z5 reached 80%, indicating that most of the micropores were blocked by carbon deposition. After introducing mesopores, the diffusion property of coke precursors from micropores to external surface was improved and more coke was deposited on the external surface, so the $R_{V_{\text{meso}}}$ of the samples were all higher than $R_{V_{\text{micro}}}$.

The internal and external coke contents were determined from the nitrogen physisorption and TG results. As shown in Fig. 12, for microporous Z5, the internal coke content was $0.079 \text{ g g}^{-1} \text{ cat}$, accounting for 95% of the total coke content. This is because the diffusion restraints of micropores blocked the path of coke from microporous channels to external surface, and most of the coke deposited inside the micropores. Small mesopores in Z5(1) improved the diffusion performance of coke, and the internal coke content increased to $0.11 \text{ g g}^{-1} \text{ cat}$, and the external coke content increased to $0.01 \text{ g g}^{-1} \text{ cat}$. By comparison, the mesopores of Z5(0) were larger and the external coke content increased to $0.08 \text{ g g}^{-1} \text{ cat}$. After NaOH treatment of Z5(1), the external surface area increased and the external coke content of Z5(1,0,0.3) increased to $0.1 \text{ g g}^{-1} \text{ cat}$. In contrast, the micropore surface area of Z5(1,1,0.3) increased to $234 \text{ m}^2 \text{ g}^{-1}$ and the external surface area decreased to $101 \text{ m}^2 \text{ g}^{-1}$. So more coke species were trapped in the micropores and the internal coke content reached $0.12 \text{ g g}^{-1} \text{ cat}$, while the external coke content was only $0.03 \text{ g g}^{-1} \text{ cat}$. It is also the increase in internal coke that led to a reduction in its lifetime. Interestingly, the internal coke content of all the post-treated samples was higher than that of the parent ZSM-5, which is likely to be related to the increased availability of acid sites in the micropore. Moreover,

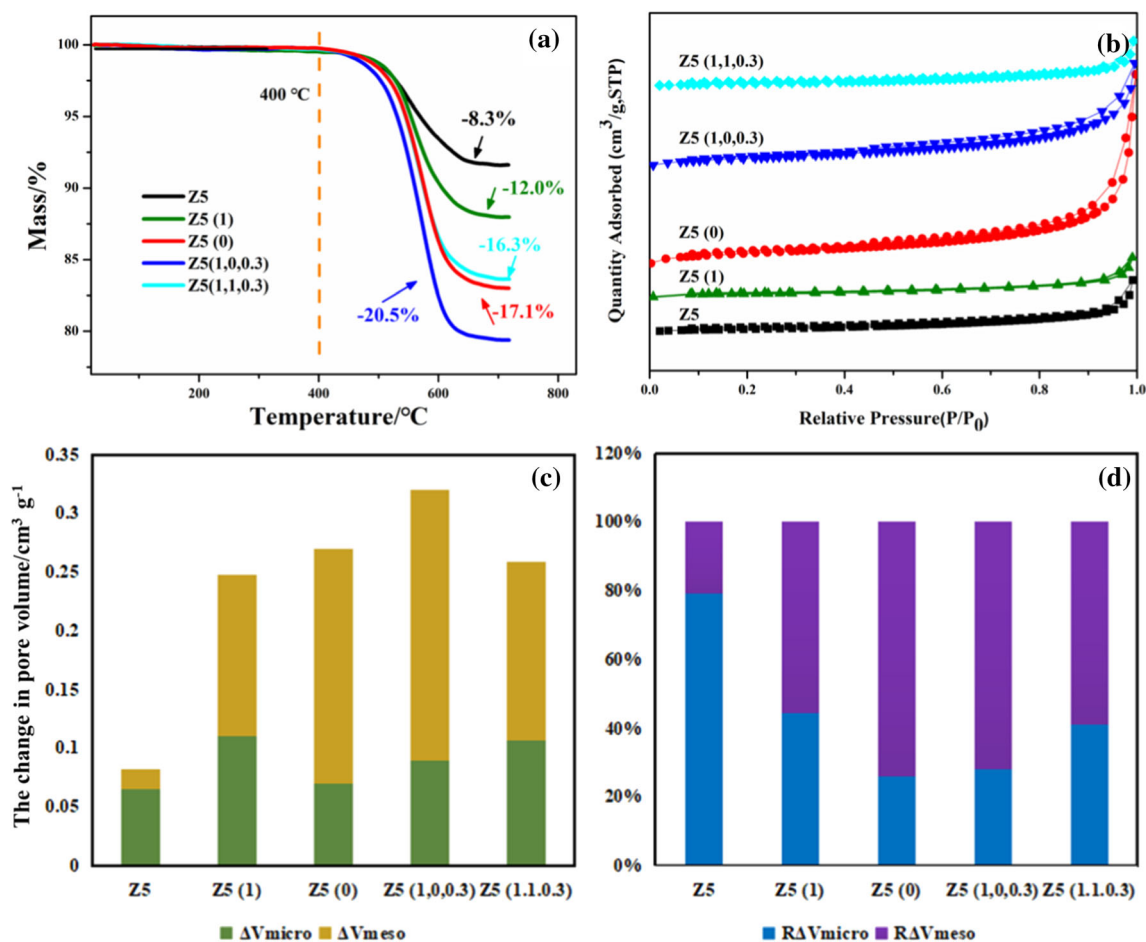


Figure 11 a TG curves, b N_2 physisorption isotherms and c, d the change and the reduction degree of micropore and mesopore volume of the spent ZSM-5 zeolites.

Table 2 Coke content and coke formation rate of the spent ZSM-5 zeolites

Samples	Lifetime (h)	Coke content ($g\ g^{-1}\ cat$)	Coke formation rate ($10^{-3}\ g\ g^{-1}\ cat\ h^{-1}$)
Z5	10	0.08	8.38
Z5(1)	22.5	0.12	5.34
Z5(0)	52.5	0.17	3.24
Z5(1,0,0.3)	58	0.21	3.62
Z5(1,1,0.3)	45	0.16	3.64

Z5(1,0,0.3) possessed more micropores and more reactions could occur in the micropores, resulting in higher internal coke content than Z5(0).

Effect of methanol space velocity on MTA reaction

Z5(0) and Z5(1,0,0.3) were evaluated at different methanol space velocity, and the influence of their pore structures on the catalytic performance was further investigated. It was found that methanol

conversion of Z5(0) and Z5(1,0,0.3) was almost 100% at different methanol space velocity (Fig. 13a, b). Increasing methanol space velocity increased the quality of effective catalyst for the conversion of methanol to C_4 + hydrocarbon, and the liquid hydrocarbon yield of Z5(0) and Z5(1,0,0.3) both increased. However, high space velocity made the contact between reactants and acid sites of zeolites insufficient and reduced the aromatic-based cycle, and aromatics, including BTX and C_9 + aromatic selectivity decreased (Fig. 13c, d). For Z5(1,0,0.3), its

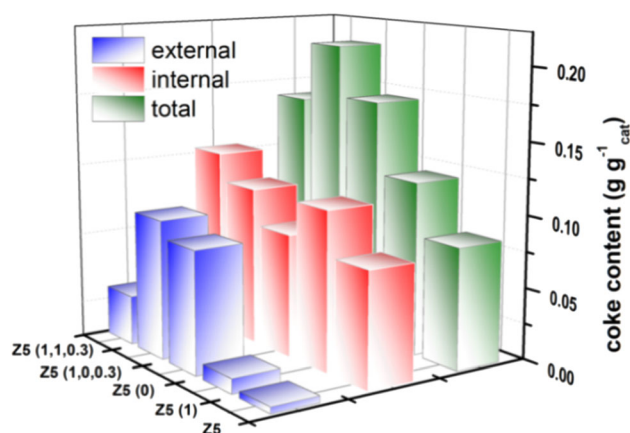


Figure 12 The comparison of the total, internal and external amount of coke in the spent ZSM-5.

large amount of strong acid sites ensured high catalytic activity, and its liquid hydrocarbon yield was higher than that of Z5(0) at each space velocity. The aromatics and BTX selectivity of Z5(1,0,0.3) were also higher than that of Z5(0), which is attributed to the increased aromatic-based cycle due to its better micropores. In order to further study the effect of space velocity on the catalytic performance of catalysts with different pore structures, the aromatics and BTX selectivity at WHSV = 2 h⁻¹ were selected as reference, and the ratio of the decrease value of aromatics and BTX selectivity at WHSV = 4 and 8 h⁻¹ to that at WHSV = 2 h⁻¹ was calculated (Fig. 13e, f). It is found that for Z5(1,0,0.3), its decrease degree of aromatic and BTX selectivity was less than that of Z5(0). This result indicated that the well-maintained micropores and strong acid sites could ensure more aromatic-based cycle to be carried out at high methanol space velocity.

Regeneration performance

Z5(0) and Z5(1,0,0.3) were selected to investigate the regeneration performance. After regeneration, the coke deposited in the catalyst was removed by calcination at high temperature, so the mesoporous property of the catalyst was partially recovered and Z5(0)-Re and Z5(1,0,0.3)-Re both presented type IV isotherms with a remarkable hysteresis loop (Fig. 14a and b). The recover degree of external and micropore surface area of Z5(0)-Re was 63% and 48%, while that of Z5(1,0,0.3)-Re was 71% and 60% (Fig. 14e). NH₃-

TPD results showed that after MTA reaction, the acid sites of the used catalyst were almost covered, and the amounts of the acid sites of Z5(0)-De and Z5(1,0,0.3)-De were both only 0.06 mmol g⁻¹. After regeneration, the acidity of the catalyst was partially recovered. Specifically, the amounts of acid sites of Z5(0)-Re recovered to 0.27 mmol g⁻¹, which accounted for 29% of Z5(0) and that of Z5(1,0,0.3)-Re recovered to 0.33 mmol g⁻¹, which accounted for 37% of that of Z5(1,0,0.3). The reduced acidity of regenerated catalysts was due to the loss of Al caused by the hydrolysis during the reaction and regeneration [50, 51]. The above high recover degree of Z5(1,0,0.3)-Re, including acidity and pore structure suggested that the well-maintained micropores of Z5(1,0,0.3) protected Al from hydrolysis to a certain extent and more acid sites were recovered.

After regeneration, the catalytic stability of the catalysts was increased attributed to the decreased amount of acid sites that slowed down the coke formation rate. It is worth noting that Z5(1,0,0.3)-Re with high recover degree of pore structure and acid property exhibited better regeneration performance. Compared with Z5(0)-Re, its lifetime further increased to 90 h, and the maximum liquid hydrocarbon yield reached 25.0%, higher than 21.8% of Z5(0)-Re.

Conclusions

In this paper, a simple and reproducible strategy named induced desilication has been proposed. ZSM-5 treated with TPAOH solution was selected for the subsequent alkali treatment, and the pre-built small mesopores promoted the uniformity to the secondary silicon leaching. The rationality of the induced mechanism was proved by alkali treatment of silicalite-1, and the inspiration was given that the flexibility of pure desilication could be realized. As a consequence, ZSM-5 zeolites with high mesoporosity and minimum micropores loss were successfully obtained. The mesopore surface area was up to 148 m² g⁻¹, and the micropore surface area still maintained at 216 m² g⁻¹. Attributed to the introduction of mesopores, long-term stability was harvested. And due to the well-maintained micropores, high liquid hydrocarbon yield and aromatic selectivity were obtained. Moreover, preliminary theoretical guidance was given on how to control the acidity of zeolites

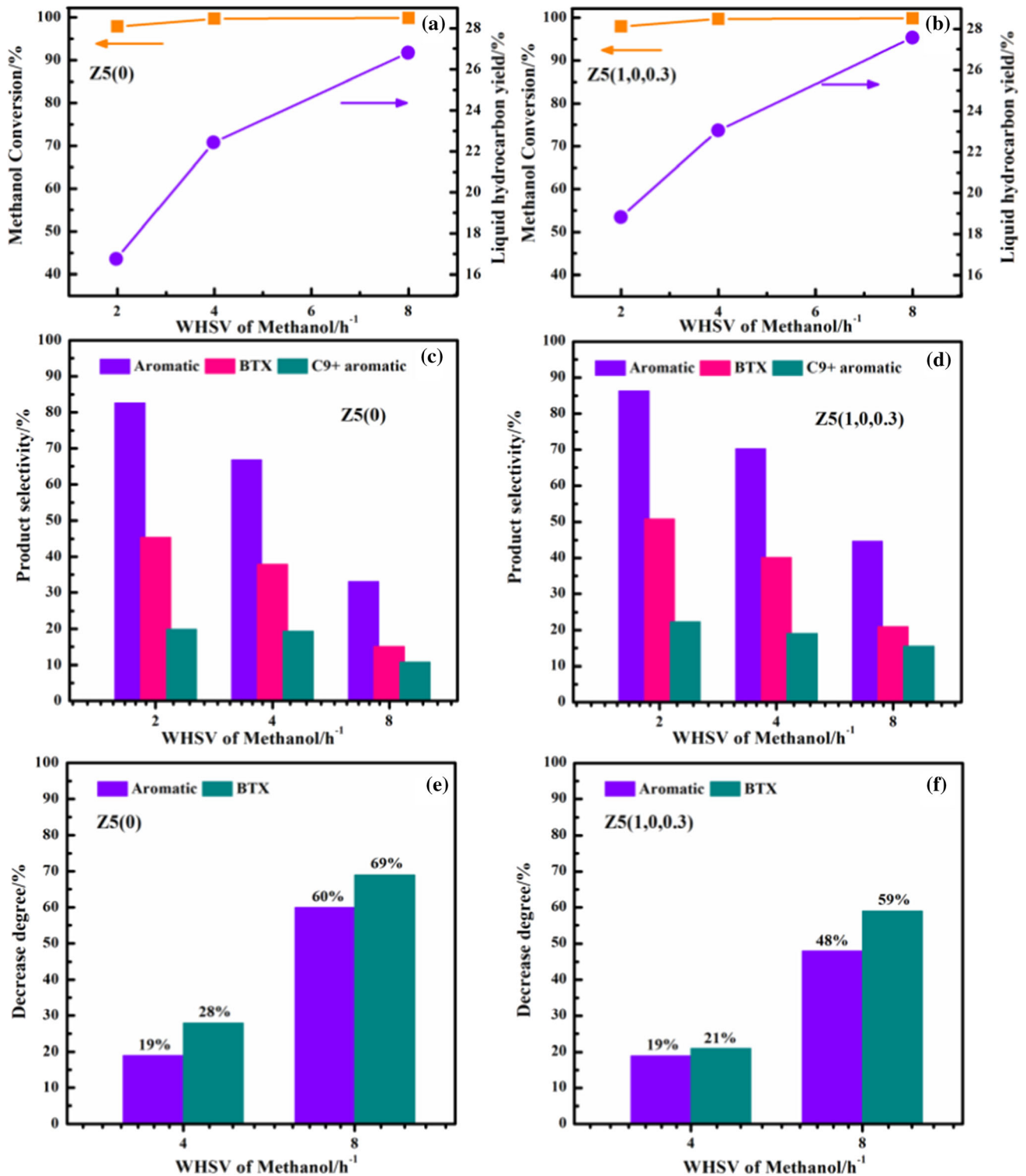


Figure 13 Effect of space velocity on methanol conversion, liquid hydrocarbon yield and production selectivity.

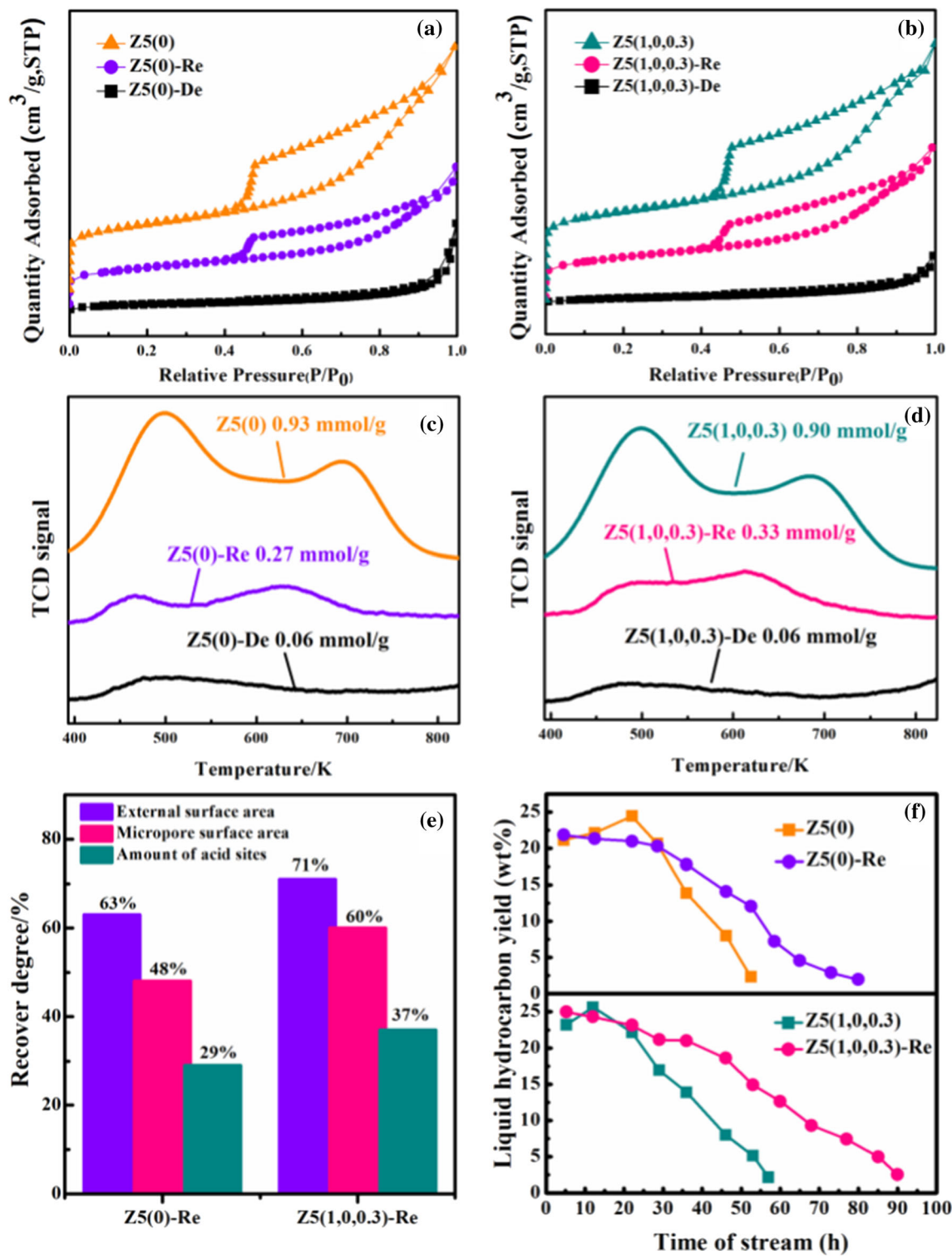


Figure 14 a, b N₂ adsorption–desorption isotherms and c, d NH₃-TPD profiles of fresh, deactivated and regenerated catalysts, e recover degree of texture properties and acidity and f liquid

hydrocarbon yield of the MTA reaction as a function of time on stream (TOS) over fresh and regenerated catalysts.

during alkali treatment. Considering the broad application of desilication, the expansion of the approach to other zeolites deserves further efforts.

Acknowledgements

We gratefully acknowledge National Natural Science Foundation of China (No.21878207, No.21978191, No.21606160), Key Research and Development Project (International Science and Technology Cooperation Program) (201803D421011) and Scientific and Technological Innovation Programs of Higher Education Institutions in Shanxi.

Compliance with ethical standards

Conflict of interest The authors declare that they have no conflict of interest.

Electronic supplementary material: The online version of this article (<https://doi.org/10.1007/s10853-020-04855-5>) contains supplementary material, which is available to authorized users.

References

- [1] Chen H, Yang M, Shang W et al (2018) Organosilane surfactant-directed synthesis of hierarchical ZSM-5 zeolites with improved catalytic performance in methanol-to-propylene reaction. *Ind Eng Chem Res* 57:10956–10966
- [2] Farneth WE, Gorte RJ (1995) Methods for characterizing zeolite acidity *Cheminform* 95:615–635
- [3] Corma A (1995) Inorganic solid acids and their use in acid-catalyzed hydrocarbon reactions. *Chem Rev* 26:559–614
- [4] Holzinger J, Beato P, Lundegaard LF et al (2018) Distribution of Aluminum over the Tetrahedral Sites in ZSM-5 Zeolites and Their Evolution after Steam Treatment. *J Phys Chem C* 122:15595–15613
- [5] Althoff R, Schulz-Dobrick B, Schüth F et al (1993) Controlling the spatial distribution of aluminum in ZSM-5 crystals. *Microporous Mesoporous Mater* 1:207–218
- [6] Irina Y, Kristof DW, Simon B (2018) Structure–performance descriptors and the role of Lewis acidity in the methanol-to-propylene process. *Nat Chem* 10:804–812
- [7] Mohamed MM, Zidan FI, Fodail MH et al (2007) Synthesis of ZSM-5 zeolite of improved bulk and surface properties via mixed templates. *J Mater Sci* 42:4066–4075. <https://doi.org/10.1007/s10853-006-0172-y>
- [8] Jiao YL, Fan XL, Perdjon M et al (2017) Vapor-phase transport (VPT) modification of ZSM-5/SiC foam catalyst using TPAOH vapor to improve the methanol-to-propylene (MTP) reaction. *Appl Catal A Gen* 545:104–112
- [9] Dai WL, Yang L, Wang CM et al (2018) Effect of n-Butanol Cofeeding on the Methanol to Aromatics Conversion over Ga-Modified Nano H-ZSM-5 and Its Mechanistic Interpretation. *ACS Catal* 8:1352–1362
- [10] Remi JCS, Lauerer A, Chmelik C et al (2015) The role of crystal diversity in understanding mass transfer in nanoporous materials. *Nat Mater* 15:401
- [11] Barakov R, Nataliya S, Pavel Y et al (2016) Low-temperature and alkali-free dual template synthesis of micro-mesoporous aluminosilicates based on precursors of zeolite ZSM-5. *J Mater Sci* 51:4002–4020. <https://doi.org/10.1007/s10853-015-9719-0>
- [12] Valtchev V, Balanzat E, Mavrodinova V et al (2011) High energy ion irradiation-induced ordered macropores in zeolite crystals. *J Am Chem So* 133:18950
- [13] Čížmek A, Subotić B, Aiello R et al (1997) Dissolution Of High-Silica Zeolites In Alkaline Solutions. 2. Dissolution Of Activated Silicalite-1 And Zsm-5 With Different Aluminum Content. *Microporous Mesoporous Mater* 8:159–169
- [14] Sano T, Nakajima Y, Wang ZB (1997) Effect of framework aluminum on the dissolution process of ZSM-5 zeolite crystal. *Microporous Mesoporous Mater* 12:71–77
- [15] Groen JC, Jansen JC, Moulijn JA et al (2004) Optimal aluminum-assisted mesoporosity development in MFI zeolites by desilication. *Cheminform* 35:13062–13065
- [16] Verboekend D, Mitchell S, Milina M et al (2011) Full compositional flexibility in the preparation of mesoporous MFI zeolites by desilication. *J Phys Chem C* 115:14193–14203
- [17] Holm MS, Svelle S, Joensen F et al (2009) Assessing the acid properties of desilicated ZSM-5 by FTIR using CO and 2,4,6-trimethylpyridine (collidine) as molecular probes. *Appl Cata A Gen* 356:23–30
- [18] Zhao L, Shen BJ, Gao JS (2008) Investigation on the mechanism of diffusion in mesopore structured ZSM-5 and improved heavy oil conversion. *J Cata* 258:228–234
- [19] Groen JC, Moulijn JA, Pérez-Ramírez J (2007) Alkaline post treatment of MFI zeolites. From accelerated screening to scale-up. *Ind Eng Chem Res* 46:4193–4201
- [20] Mochizuki H, Yokoi T, Imai H et al (2012) Effect of desilication of H-ZSM-5 by alkali treatment on catalytic performance in hexane cracking. *Appl Catal A Gen* 449:188–197
- [21] Li HZ, Dong LX, Zhao L et al (2017) Enhanced adsorption desulfurization performance over mesoporous ZSM-5 by alkali treatment. *Ind Eng Chem Res* 56:3813–3821

- [22] Wang J, Zhong ZP, Ding K et al (2017) Successive desilication and dealumination of HZSM-5 in catalytic conversion of waste cooking oil to produce aromatics. *Energ Convers Manage* 147:100–107
- [23] Wang DR, Zhang L, Chen L et al (2014) Postsynthesis of mesoporous ZSM-5 zeolite by piperidine-assisted desilication and its superior catalytic properties in hydrocarbon cracking. *J Mater Chem A* 3:3511–3521
- [24] PÄ©rez-RamÄ©rez J, Verboekend D, Bonilla A et al (2009) Zeolite catalysts with tunable hierarchy factor by pore-growth moderators. *Adv Funct Mater* 19:3972–3979
- [25] Sadowska K, Wach A, Olejniczak Z et al (2013) Hierarchic zeolites: Zeolite ZSM-5 desilicated with NaOH and NaOH/tetrabutylamine hydroxide. *Microporous Mesoporous Mater* 167:82–88
- [26] Qiao K, Shi X, Zhou F et al (2017) Catalytic fast pyrolysis of cellulose in a microreactor system using hierarchical zsm-5 zeolites treated with various alkalis. *Appl Catal A Gen* 547:274–282
- [27] Wan WL, Fu TJ, Qi RY et al (2016) Coeffect of Na⁺ and Tetrapropylammonium (TPA⁺) in Alkali Treatment on the Fabrication of Mesoporous ZSM-5 Catalyst for Methanol-to-Hydrocarbons Reactions. *Ind Eng Chem Res* 55:13040–13049
- [28] Ma Z, Fu TJ, Wang YJ et al (2019) Silicalite-1 Derivational Desilication-Recrystallization to Prepare Hollow Nano-ZSM-5 and Highly Mesoporous Micro-ZSM-5 Catalyst for Methanol to Hydrocarbons. *Ind Eng Chem Res* 58:2146–2158
- [29] Guisnet M, Magnoux P (2001) Organic chemistry of coke formation. *Appl Catal A Gen* 212:83–96
- [30] Bibby DM, Milestone NB, Patterson JE et al (1986) Coke formation in zeolite ZSM-5. *J Catal* 97:493–502
- [31] Wan ZJ, Kevin Li G, Wang CF et al (2018) Relating coke formation and characteristics to deactivation of ZSM-5 zeolite in methanol to gasoline conversion. *Appl Catal A Gen* 549:141–151
- [32] Abell S, Bonilla A, Prez-Ramrez J (2009) Mesoporous ZSM-5 zeolite catalysts prepared by desilication with organic hydroxides and comparison with NaOH leaching. *Appl Catal A Gen* 364:191–198
- [33] Helmkamp MM, Davis ME (1995) Synthesis of porous silicates. *Annu Rev Mater Sci* 25:161
- [34] Groen JC, Perez-Ramirez J (2004) Critical appraisal of mesopore characterization by adsorption analysis. *Appl Catal A Gen* 268:121–125
- [35] Milina M, Mitchell S, Crivelli P et al (2014) Mesopore quality determines the lifetime of hierarchically structured zeolite catalysts. *Nat Commun* 5:3922
- [36] Groen JC, Peffer LA, Moulijn JA et al (2005) Mechanism of hierarchical porosity development in MFI zeolites by desilication: The role of aluminium as a pore-directing agent. *Chemistry* 11:4983–4994
- [37] Fodor D, Belouqui Redondo A, Krumeich F et al (2015) Role of defects in pore formation in MFI zeolites. *J Phys Chem C* 119:5447–5453
- [38] Li T, Ihli J, Ma Z et al (2019) Composition and Structure Dependent Mesopore/Macropore Formation in Zeolites by Desilication. *J Phys Chem C* 123:8793–8801
- [39] Feng Z, Yan G, Wu G et al (2017) Improved catalytic performance and decreased coke formation in post-treated ZSM-5 zeolites for methanol aromatization. *Microporous Mesoporous Mater* 240:96–107
- [40] Yang ST, Yu CX, Yu LL et al (2017) Bridging dealumination and desilication for the synthesis of hierarchical MFI zeolites. *Angew Chem Int Ed* 56:12553–12556
- [41] Xin HC, Li XP, Fang Y et al (2014) Catalytic dehydration of ethanol over post-treated ZSM-5 zeolites. *J Catal* 312:204–215
- [42] Hao C, Wang QF, Zhang XW et al (2015) Quantitative conversion of triglycerides to hydrocarbons over hierarchical ZSM-5 catalyst. *Appl Catal B* 166–167:327–334
- [43] Hartmann M (2004) Hierarchical zeolites: A proven strategy to combine shape selectivity with efficient mass transport. *Angew Chem Int Ed Engl* 43(44):5880–5882
- [44] Zhang CD, Kawk G, Lee YJ et al (2019) Light hydrocarbons to BTEX aromatics over Zn-modified hierarchical ZSM-5 combined with enhanced catalytic activity and stability. *Microporous Mesoporous Mater* 284:316–326
- [45] Zhang JG, Qian WZ, Kong CY et al (2015) Increasing para-Xylene Selectivity in Making Aromatics from Methanol with a Surface-Modified Zn/P/ZSM-5 Catalyst. *ACS Catal* 5:2982–2988
- [46] Miyake K, Hirota Y, Ono K et al (2016) Direct and selective conversion of methanol to para-xylene over Zn ion doped ZSM-5/silicalite-1 core-shell zeolite catalyst. *J Catal* 342:63–66
- [47] Arian G, Abhishek G, Grabow LC et al (2015) Epitaxial growth of ZSM-5@ Silicalite-1: A core-shell zeolite designed with passivated surface acidity. *ACS Nano* 9:4006–4016
- [48] Schmidt F, Hoffmann C, Giordanino F et al (2013) Coke location in microporous and hierarchical ZSM-5 and the impact on the MTH reaction. *J Catal* 307:238–245
- [49] Kim J, Choi M, Ryoo R (2010) Effect of mesoporosity against the deactivation of MFI zeolite catalyst during the methanol-to-hydrocarbon conversion process. *J Catal* 269:219–228

- [50] Campbell SM, Bibby DM, Coddington JM et al (1996) Dealumination of HZSM-5 Zeolites I. Calcination and Hydrothermal Treatment I. *J Catal* 161:338–349
- [51] Campbell SM, Bibby DM, Coddington JM et al (1996) Dealumination of HZSM-5 Zeolites II. Methanol to gasoline conversion I. *J Catal* 161:350–358

Publisher's Note Springer Nature remains neutral with regard to jurisdictional claims in published maps and institutional affiliations.